Effect of Air Inlet Speed Variations on Oil Palm Loose Fruit Collector

Adam Danial Lim Jefri Lim[a,d]*, Saiful Anuar Abu Bakar[a,c]**, Mohd Faridh Ahmad Zaharuddin[b], Mohd Farid Muhamad Said[c]
[a]*Department of Aeronautics, Automotive and Ocean Engineering, Faculty of Mechanical Engineering, Universiti Teknologi Malaysia, 81310 Skudai, Johor, Malaysia.*
[b]*Department of Manufacturing and Industrial Engineering, Faculty of Mechanical Engineering, Universiti Teknologi Malaysia, 81310, Skudai, Johor, Malaysia*
[c]*Automotive Development Centre, Institute of Vehicle Systems and Engineering, Universiti Teknologi Malaysia, 81310, Skudai, Johor, Malaysia*
[d]*Department of Agricultural and Biosystems Engineering, Faculty of Engineering, Universiti Putra Malaysia, 43400, Serdang, Selangor, Malaysia.*

Abstract

Oil palm is one of the largest economic sectors in Malaysia. Among the problems faced in the estates is oil palm loose fruit deposition, which is currently being collected manually in the industry. Hence, an oil palm loose fruit collector was designed using a cyclone separator mechanism and was studied using computational fluid dynamics (CFD). In the current study, Reynold's stress model (RSM) and the discrete phase model (DPM) were employed to navigate numerical simulations where air speed intake of the designed machine was varied at 13, 30, and 46 m/s, respectively. The wall was set to a no-slip condition with standard wall functions. The hydraulic diameter of the gas outlet was B_c = 0.1 m. The hydraulic diameters of the particle's outlet were J_c = 0.15 m and 0.2 m, respectively. Turbulence intensity at the gas and particle outlet was specified at 5%. An injection with density of 995.7 kg/m^3 and a diameter of 0.04 m was set to simulate oil palm loose fruit collection into the system. Effects of air speed variations on the pressure drop and collection efficiency were then analyzed. It was found that increasing the inlet air speed from 13 m/s to 30 m/s reduced the collection efficiency by 14.92 % from 80.05% to 66.13%, while a 54.444% collection was recorded at 46 m/s inlet air speed. Ultimately, results indicate that a lower air speed is favorable in terms of pressure drop and collection efficiency.

Keywords: *Computational fluid dynamics, Cyclone separator, Discrete phase model, Oil palm loose fruits, Reynold's stress model*

1. Introduction

Oil palm is one of the main agricultural crops planted in Malaysia, covering 5,652,569 hectares of land in the nation as of 2023. From the total planted area, 73.5% is of plantations managed by private and government estates, 14.9% belongs to independent small holders, and the remaining 11.9 % belongs to organized small holders [1]. In general, the oil palm industry is categorized into

* Corresponding author.
E-mail address: saifulanuar@utm.my

Manuscript History:
Received 21 March, 2024, Revised 30 September, 2024, Accepted 1 October, 2024, Published 31 October, 2024

https://doi.org/10.33736/jaspe.6822.2024

e-ISSN: 2289-7771

upstream and downstream divisions. The upstream comprises activities conducted in plantations and transportation to the palm mills, whereas downstream activities begin in the mill. According to Yusoff *et al*. [2], the activities involved upstream in plantations are cutting fresh fruit bunches, frond stacking, fresh fruit bunch collection, loose fruit collection, and lastly transportation of harvests to the mill. Generally, the reason to collect oil palm loose fruits is to avoid losses, as the fruits produce a high oil extraction rate (OER) due to their ripeness [3–4]. Sime Darby [5] stated that the OER per weight ratio of loose fruits stands at 40 %, while Shuib *et al*. [6] stated that the outer layer of bunches gives out almost 50 % of the total oil percentage in a bunch. Therefore, if loose fruits are not collected, the total OER of fruit bunches will drop as the portions that make up the highest OER are not included. This is further supported by Chang *et al*. [7], who reported loose fruit collection as one of the factors directly affecting OER. The current method of collection involves manual labor, using rakes to collect the fruits and placing them in bags for transportation by wheelbarrows [8–9]. However, the implementation of loose fruit collection using the current method entails some negative effects. Firstly, the manual rake and bag method introduces a substantial amount of debris. Ahmad *et al*. [10], Darius & Fairulnizam [4] and Yusoff *et al*. [8] reported debris of 60%, 30-40 % and 20-30%, respectively. A high percentage of debris will lower OER [11]. As a solution, Shuib & Khalid [12] introduced a separating machine to clear debris from the manually collected fruits. The machine, however, only solves the problem of debris clearing but not the other shortcomings of manual collection. Hence, an oil palm loose fruit collector is designed using the cyclone separator mechanism to address the disadvantages of manual collections.

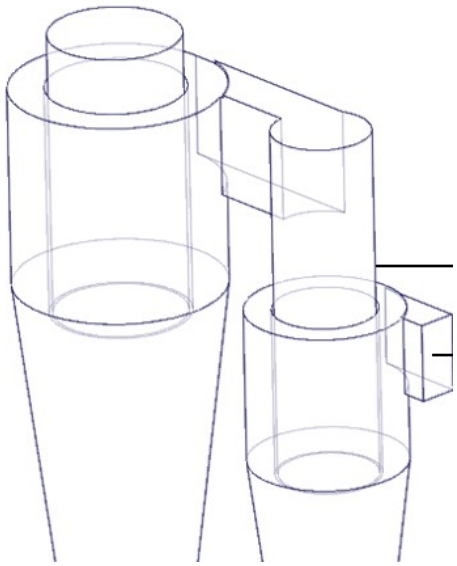

Figure 1. Designed cyclone separator used in study.

The principle of the designed cyclone separator, as shown in Figure 1, boasts a dual cyclone separator system that acts as a separating mechanism for oil palm loose fruit and debris as they are gathered via air suction. Oil palm loose fruit will be introduced into the smaller first-stage cyclone separator as the loose fruits are collected via air suction through the inlet. Heavy, loose fruits will be gathered via the outlet in the first-stage cyclone separator, while lighter debris will be pulled through the vortex finder and collected in the second-stage cyclone separator. Clean, loose fruits will thus be collected by the first-stage cyclone, while undesirable debris will be deposited in the second-stage cyclone.

The design of cyclone separators is generally simple with minimal maintenance and variable working temperature, which is the main reason it is opted by the industry as a method for material separation [13]. According to Park and Go [14], the working principle of the air cyclone separator is that as materials are being sucked in through the inlet, a centrifugal force will act on the materials, which forces them to the separator walls, while the drag force acting on the materials forces them to the center of the cyclone separator. Thus, heavy or course materials will remain on the walls, swirling down to be collected via the outer vortex of the cyclone separator, while lighter fine materials that have been dragged to the center of the cyclone where the inner vortex is located, will be transported out of the system.

There are various parts of the cyclone separator regarded as critical to its performance. One of the most extensively studied parts is the inlet. A study by Babaoglu et al. [15] revealed that the rectangle-rectangle configuration of inlet shapes for double inlet cyclone separators contributed to the maximum tangential velocity. The most efficient configuration in terms of collection is the rectangular eclipse. The cyclone separators are designed such that the cross-sectional area ratio of the primary inlet to the secondary is 0.069. Shapes that were studied include the circle, ellipse, rectangle, square, and trapezoid, which gave a total of 25 combinations of configurations. Gao *et al*. [16] studied three distinct types of inlet structures in a cyclone's separator flow field. Through numerical simulations, it was found that the AVI type had better performance in terms of cyclone vorticity, where the vortex was also more uniform and stable compared to STI and SVI. In another study, Nassaj *et al*. [17] designed guide channels for multi-inlet cyclone separators to evaluate the cyclone performance of conventional cyclones. The study resulted in the conclusion that the guide channels increased the inlet velocity of the cyclone, also having better performance than conventional cyclones in terms of pressure and velocity distributions. It was also reported that a 20% decrease in inlet velocity also decreased the tangential velocity by up to 35% but resulted in improved particle separation efficiency. Siadaty *et al*. [18] studied temperature variations at the inlet and found that raising the temperature reduced the vortex strength, resulting in a decrease in performance. Misiulia *et al*. [19] developed a helical-roof inlet cyclone separator and intended to study the effects of a cyclone. Misulia *et al*. [20] found that raising the inlet angle would result in cyclone cut size reduction, which in turn would reduce collection efficiency, while inlet angle 10-15 was found to be the optimum angle. This study was a continuation of a previous study in 2015 [21], where they found that a cyclone separator roof with a helical inlet gave better aerodynamic efficiency. Wasilewski and Duda *et al*. [22] worked on varying inlet angles and other design criteria such as the type of gas inlet and outlet. They found that raising the inlet angle and reducing the gas outlet length had the most significant effect on the performance of a cyclone separator. On another note, Liu *et al*. [23] found that multi-inlet cyclones operated at a higher aerosol flow than one-inlet cyclone separators. In 2010, Elsayed and Lacor [24] worked on varying conventional inlet dimensions on their heights and widths by ratio and found that the best ratio was 0.5-0.7, where the conventional cyclone separator had a value of 0.5. Hence, a conclusion can be obtained from the information in the literature review: the inlet of a cyclone separator serves as an important parameter in design considerations. In the context of designing an efficient oil palm loose fruit separator, previous designs of suction methods and air speeds were studied, as shown in Table 1.

Table 1. Summary of suction type oil palm loose fruit collection machine.

Reference	Concept	Air velocity ($m\ s^{-1}$)	Debris (%)
Ahmad et al. [10]	Direct suction with in line separator	n.a.	10
Ahmad et al. [25]	Direct suction with in line separator	20-35	n.a.
Shuib et al. [26]	Cyclonic vacuum with separation mechanism	n.a.	<15
Shuib et al. [27]	Tractor's PTO shaft operated cyclonic	40	7.5

	vacuum		
Yusoff et al. [28]	Direct suction, built-in rotating separator and tipping bin	n.a.	5-10

*n.a. = not available

Referring to Table 1, the machines developed using the suction method generally had low percentages of debris compared to the manual method, where debris ranged from 20–60%. It is also evident that the suction mechanism had been improved, with the MK III [12] utilizing a cyclonic vacuum concept over direct suction methods by Ahmad et al. [10] & [26] to address choking issues along the suction line. Ramdhan et al. [27] experimented on the MK III and found that an air speed of 22.4 m/s with an air flow of 0.21 m3/s was the minimum requirement to suck one loose fruit into the system. Several loose fruits would require air speed between 30 m/s to 35 m/s. Other suggestions from the experiment include minimization of fitting installations and using a more robust yet light material for the blower to resist impacts. However, if fruits filled up more than 50% of the chamber in MK III, trash might not be blown out due to a reduction in air flow [12]. This occurrence woud in turn jeopardize the debris separation system. Yusoff et al. [26] then proceeded with direct suction but chose to exclude the separation mechanism from the pressure line. In this particular study, the inlet air speed was studied to assess its effects on the collection efficiency of the designed machine. In order to do this, computational fluid dynamics (CFD) was employed to further analyze the flow in the system.

In performing computations using CFD, firstly, a suitable model must be chosen to navigate the simulation. This step is crucial in order to generate accurate results in observing flow in the cyclone separator. The fact that the flow in a cyclone separator is rather complex and is turbulent also gives a variety of choices of turbulent models to choose from. Other turbulent flow selections available are Reynold's Stress Model (RSM), Large Eddy Simulation (LES) Model, Detached Eddy Simulation (DES) Model and the k-ε model. Generally, RSM is opted over LES because it uses less computational time with satisfactory, accurate results. Moreover, a study conducted by Hoekstra [28], who numerically simulated and performed experimental validation on the cyclone separator using several turbulence models, found that only the RSM can successfully characterize the flow of cyclones accurately. Hence, RSM is the most suitable model for simulating the dual cyclone separator and loose fruit collector. In considering particle injection, DPM is favored by most of the literature. The basis for the selection is explained by the Ansys Fluent Theory Guide [29], where DPM is suitable for tracking particle-bearing flows in which the dispersion occupies a low volume fraction and where collisions between particles can be ignored. This particular condition has made DPM viable and satisfactory for numerical simulations, as the separation mechanism of particles in a cyclone separator follows the aforementioned condition.

2. Methodology

2.1. Governing equations of the RSM

According to Ansys Fluent Theory Guide [29], RSM navigates the Reynolds-averaged Navier-Stokes (RANS) equations by solving the Reynolds stresses' transport equations alongside a dissipation rate equation. The model approaches the effects of streamlined curvature, swirl, rotation and also rapid variations in strain rates thoroughly, making the model essential in simulating cyclone flows.
The Reynolds stresses' transport equation is given as such:

$$\frac{\partial}{\partial t}(\rho_f \overline{u'_i u'_j}) + C_{ij} = D_{T,ij} + D_{L,ij} + P_{ij} + G_{ij} + \phi_{ij} + \varepsilon_{ij} + F_{ij} + S_u \quad (1)$$

where $\frac{\partial}{\partial t}(\rho_f \overline{u'_i u'_j})$ is the unsolved part of the RANS equation in tensor form, while C_{ij} , $D_{T,ij}$, $D_{L,ij}$, P_{ij} , G_{ij} , ϕ_{ij} , ε_{ij} , F_{ij} , S_u are the terms for equations of convection, turbulent diffusion, molecular diffusion, stress production, buoyancy production, pressure strain, dissipation, system rotation production and user-defined source respectively.

In short, RSM functions to model and compute the unsolved equation, $\frac{\partial}{\partial t}(\rho_f \overline{u'_i u'_j})$ as shown in Equation (1) by solving the transport and dissipation equations. In producing the RANS equation, Reynolds Averaging is applied to the Navier-Stokes equation, resulting in:

$$\frac{\partial \rho}{\partial t} + \frac{\partial}{\partial x_i}(\rho u_i) = 0 \tag{2}$$

and

$$\frac{\partial}{\partial t}(\rho u_i) + \frac{\partial}{\partial x_j}(\rho u_i u_j) = -\frac{\partial p}{\partial x_i} + \frac{\partial}{\partial x_j}\left[\mu\left(\frac{\partial u_i}{\partial_{xj}} + \frac{\partial u_j}{\partial_{xi}} - \frac{2}{3}\delta_{ij}\frac{\partial u_l}{\partial xl}\right)\right] \tag{3}$$

$$+\frac{\partial}{\partial t}(\rho_f \overline{u'_i u'_j}) \tag{4}$$

where equations (2) and (3) are the RANS equations while equation (4) is the resulting effects of turbulence to be solved by RSM.

Turbulent Diffusion, $D_{T,ij}$

Going deeper into how RSM solves equation (1) through its model, $D_{T,ij}$ is modelled by Ansys Fluent using an equation of scalar turbulent diffusivity. The equation is given as:

$$D_{T,ij} = \frac{\partial}{\partial x_k}\left(\frac{\mu_t}{\sigma_k}\frac{\partial \overline{u'_i u'_j}}{\partial x_k}\right) \tag{5}$$

where σ_k = 0.82 and the turbulent viscosity, μ_t is calculated using the exact formula used in the k-ε model:

$$\mu_t = \rho C_\mu \frac{k^2}{\varepsilon} \tag{6}$$

where C_μ − 0.09, note that this constant used in RSM does not equal the value used for k-ε models.

Pressure-Strain, ϕ_{ij}

In Ansys Fluent, the pressure-strain term is calculated and modelled automatically by the governing equation:

$$\phi_{ij} = \phi_{ij,1} + \phi_{ij,2} + \phi_{ij,w} \tag{7}$$

where $\phi_{ij,1}$, $\phi_{ij,2}$ and $\phi_{ij,w}$ are the slow pressure-strain term, rapid pressure-strain term and wall reflection term respectively.

RSM approaches the slow pressure-strain term, $\phi_{ij,1}$ by default using the equation:

$$\phi_{ij,1} = -C_1\rho\frac{\varepsilon}{k}\left(\overline{u'_i u'_j} - \frac{2}{3}\delta_{ij}k\right) \quad (8)$$

where C_1 is constant 1.8.

On the other hand, the rapid pressure-strain term $\phi_{ij,2}$ is modelled by the equation:

$$\phi_{ij,2} = -C_2\left[\left(P_{ij} + F_{ij} + \frac{5}{6}G_{ij} - C_{ij}\right) - \frac{2}{3}\delta_{ij}\left(P + \frac{5}{6}G - C\right)\right] \quad (9)$$

where C_2 is 0.6, C is $0.5C_{kk}$ while P_{ij}, F_{ij}, G_{ij} and C_{ij} is as explained in equation (1).

The final term of the pressure-strain term which is the wall reflection term, $\phi_{ij,w}$ is rather complex as it functions to redistribute the normal stresses near the wall. The term is modelled using the equation:

$$\phi_{ij,w} = C'_1\frac{\varepsilon}{k}\left(\overline{u'_k u'_m}\, n_k n_m \delta_{ij} - \frac{3}{2}u'_i u'_k\, n_j n_k - \frac{3}{2}u'_j u'_k\, n_i n_k\right)\frac{C_l k^{\frac{3}{2}}}{\varepsilon d}$$

$$+ C'_2\left(\phi_{km,2} n_k n_m \delta_{ij} - \frac{3}{2}\phi_{ik,2} n_j n_k - \frac{3}{2}\phi_{jk,2} n_i n_k\right)\frac{C_l k^{\frac{3}{2}}}{\varepsilon d} \quad (10)$$

where C'_1 is 0.5, C'_2 is 0.3, $C_l = C_\mu^{\frac{3}{4}}$ where C_μ is 0.9, k is the von Karman constant with the value of 0.4187 while n_k and d is the $x_k$component of the unit and distance normal to the wall respectively

Buoyancy Production, G_{ij}

The effects of buoyancy modelled in the RSM turbulent model are governed by the equations:

$$G_{ij} = -\rho\beta\left(g_i\overline{u'_j\theta} + g_j\overline{u'_i\theta}\right) \quad (11)$$

$$\overline{U_i\theta} = \frac{\mu_t}{Pr_t}\left(\frac{\partial T}{\partial x_i}\right) \quad (12)$$

where the Prandt number, Pr_t =0.85, which is the turbulent number for energy and β stands for the coefficient of thermal expansion which is further elaborated by the equation:

$$\beta = -\frac{1}{\rho}\left(\frac{\partial\rho}{\partial T}\right)_p \quad (13)$$

Solving equation (13) for buoyancy production in ideal gases, the following equation is obtained and modelled for RSM:

$$G_{ij} = -\frac{\mu_t}{Pr_t}\left(g_i\frac{\partial\rho}{\partial x_j} + g_j\frac{\partial\rho}{\partial x_i}\right) \quad (14)$$

Dissipation, ε_{ij}

In RSM, the dissipation rate in a turbulent system is modelled using the equation:

$$\varepsilon_{ij} = \delta_{ij}(\rho\varepsilon + Y_M) \quad (15)$$

where Y_M is the additional dilatation dissipation and ε is the scalar dissipation rate. It can be solved using the following expression:

$$Y_M = 2\rho\varepsilon M_t^2 \tag{16}$$

where M_t is defined as the Mach number and can be calculated using the formula:

$$M_t = \sqrt{\frac{k}{a^2}} \tag{17}$$

where a is the speed of sound. The scalar dissipation rate, ε which is present in both equations (15) and (16) is solved using the same transport equation used in the k- ε model. The equation is as follows:

$$\frac{\partial}{\partial t}(\rho\varepsilon) + \frac{\partial}{\partial x_i}(\rho\varepsilon u_i) = \frac{\partial}{\partial x_j}\left[\left(\mu + \frac{\mu_t}{\sigma_\varepsilon}\right)\frac{\partial\varepsilon}{\partial x_j}\right] + C_{\varepsilon 1}\frac{\varepsilon}{k}[P_{ii} + C_{\varepsilon 3}G_{ii}] - C_{\varepsilon 2}\rho\frac{\varepsilon^2}{k} + S_\varepsilon \tag{18}$$

where σ_ε, $C_{\varepsilon 1}$ and $C_{\varepsilon 2}$ is 1.0, 1.44 and 1.92 respectively while $C_{\varepsilon 3}$ is computed as a function of local flow direction relative to gravitational vector. S_ε is denoted as a user-defined source term.

2.2. Discrete phase model

In general, the discrete phase model (DPM) and multiphase model are two methods for calculating particle-laden flows in a fluid using CFD. DPM was chosen because the second injected phase only constitutes a small percentage of volume, and if the case indicates otherwise, the multiphase model should be used. Therefore, we can disregard the interactions between the particles and use DPM to calculate their interactions within the fluid flow. The governing equations of DPM follow the Euler-Langrage approach, where the fluid phase is treated as a continuum in solving the Navier-Stokes equations. In DPM, the trajectory of a single particle is governed numerically by equating its inertia to the forces acting on it. The equation is given as follows:

$$\frac{d\vec{u_p}}{dt} = F_D(\vec{u} - \vec{u_p}) + \frac{\vec{g}(\rho_p - \rho)}{\rho_p} + \vec{F} \tag{19}$$

where $\vec{u}$ = fluid phase velocity, $\vec{u_p}$ = particle velocity, μ = molecular velocity of the fluid, ρ = density of the fluid, ρ_p = density of particle, $\vec{F}$ = additional acceleration, force per unit particle mass and $F_D(\vec{u} - \vec{u_p})$ = drag force per unit particle mass which can be further elaborated by the equation:

$$F_D = \frac{18\mu\, C_D Re}{\rho_p d_p^2\, 24} \tag{20}$$

where d_p = particle diameter and Re, the Reynolds number can be represented by the formula:

$$Re = \frac{\rho d_p|\vec{u_p} - \vec{u}|}{\mu} \tag{21}$$

while C_D, the drag coefficient from equation (20) is given by the formula, for spherical drag:

$$C_D = a_1 + \frac{a_2}{Re} + \frac{a_3}{Re^2} \tag{22}$$

where a_1, a_2 and a_3 are constants given by Morsi & Alexander [30].

2.3. Numerical model validation

The cyclone geometry of Hoekstra's work [28] was replicated to determine the extent of accuracy the numerical model offers in developing an oil palm loose fruit collector. Pressure drop validation was performed by simulating the numerical model at velocities of 5, 7, 9, 10, 15, 18, and 20 This step ensures the solver settings in the numerical study behave accurately and demonstrate reliable precision. Figure 2 shows a comparison of the numerical simulation to experimental work where the pressure drops were measured across varied inlet velocities using pressure differential sensors. As can be seen, the simulated data is in good agreement with experimental data, where the maximum percentage difference compared to experimental data was recorded at 7.5%.

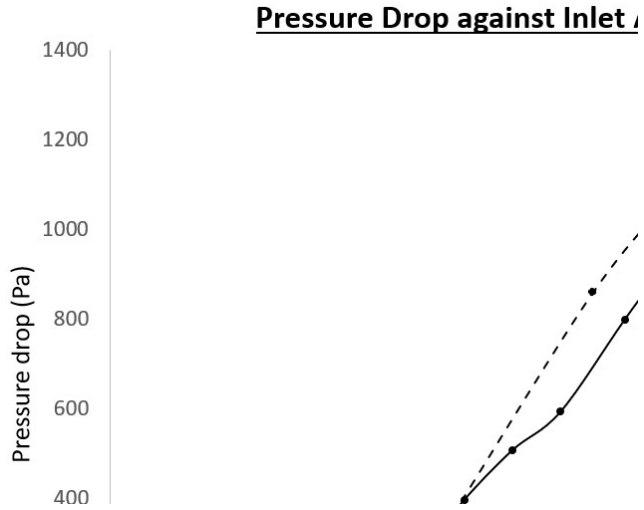

Figure 2: Pressure drop comparison between numerical simulation and experimental data.

Tangential velocity is an imperative indication of cyclone separator performance. In Figure 3, it can be seen that the experimental data [28] and the simulated data from the present study exhibited the same pattern with minor deviations. The maximum error recorded was 14.98% in the profile at a radial position of 0.58. However, for other regions, the errors were very minimal and this showed that the numerical simulation obeys the cyclone separator mechanism as validated by experimental data. Verily, precisely close comparisons of the numerical study data with the works of Hoekstra are indications that the present work is consistent and of reasonable precision.

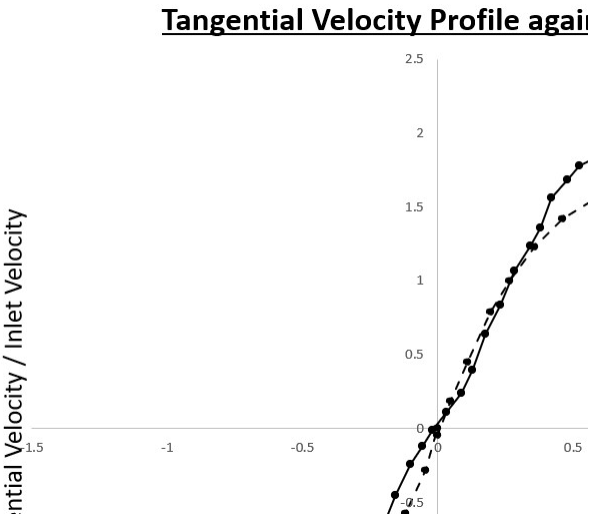

Figure 3: Tangential velocity comparison between numerical simulation and experimental data.

2.4. Cyclone geometry

The type of cyclone separator is an important design consideration, as the swirl in the cyclone will affect their collection performance due to the difference in flow characteristics. In this study, several types of cyclone separators have been considered: 1D2D, 2D2D, and 1D3D cyclone separators. El-Emam *et al*. [31] investigated the performance of various cyclone separators and discovered that the 1D2D cyclone was the most effective among conventional cyclones. The first 'D' represents the cyclone's critical diameter, while the second 'D' denotes the cyclone's height. A 1D2D cyclone separator will have a cyclone height double that of. Figure 1 provides a standard cyclone with its denoted parts, which was determined through the classical cyclone design (CCD) process as explained by Wang [32]. The following are the steps involved in determining the design basis for the cyclone separator.

$$Dc = \sqrt{\frac{8Q}{V_i}} \tag{23}$$

Where Q is air flow rate (m^3) and V_i is inlet velocity (ms^{-1})

Foremostly, the air speed and air flows needed to be determined to calculate the critical diameter, D_c. In a study conducted by Ramdhan et al. [27], the range of air velocity and air flow suggested for collecting oil palm loose fruits via suction were 30–35 and 0.28–0.33, respectively. Applying the data reported from [27] in Eqn. 23 gave a cyclone separator diameter of 0.3 m. Thus, the first cyclone was designed at a critical diameter, D_c, of 0.3 m, while the other dimensions of the first smaller cyclone separator followed the standard dimensions for 1D2D cyclone separators as shown in Figure 4. The second bigger cyclone separator was designed to have a bigger pressure drop in order to trap more materials due to its higher pressure drop. Since the total height of the system is also a concern as the system is intended to be attached to a ground vehicle, the height must also be reasonable. Hence, D_c = 0.4 m was chosen as a preliminary design for the second cyclone separator. Thus, making the maximum height of the system stood at 1.2 m tall.

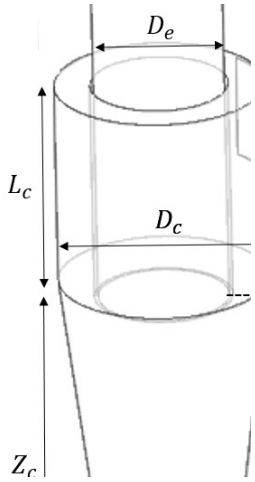

Figure 4: Standard cyclone separator.

2.5. Boundary Condition

Table 2: CFD solver settings used in the study.

Setting	**Input**
Gravity	9.81 m s-^{2}
Solver	Pressure based
Velocity formulation	Absolute
Time	Steady
Pressure-velocity coupling	SIMPLE
Spatial discretization (Pressure)	Second order
Spatial discretization (Momentum)	Second order upwind
Spatial discretization (Turbulent Kinetic Energy)	Second order upwind
Spatial discretization (Turbulent dissipation Energy)	Second order upwind
Spatial discretization (Energy)	Second order upwind

Numerous inlet velocities of 13, 30, and 46 m/s were used. RSM and DPM were used to simulate the cyclone flow field and loose fruit collection. The wall was set to a no-slip condition with standard wall functions. The hydraulic diameter of the gas outlet was Bc = 0.1. The hydraulic diameters of the particle's outlet were Jc = 0.15 and 0.2, respectively. Turbulence intensity at the gas and particle outlet was specified at 5%. For the DPM, an injection with densities of 995.7 and 0.04 was set to simulate oil palm loose fruit collection into the system [33]. Table 2 shows the solver settings used in the CFD.

Table 3: Dimensions of designed cyclone

Dimensions	First cyclone separator (mm)	Second cyclone separator (mm)
D_c	300	400
B_c	75	100
D_e	187.5	250
H_c	150	200
J_c	150	200
S_c	187.5	250
L_c	300	400
Z_c	600	800

Figure 1 depicts the design of a two-stage cyclone separator used in the study with its dimensions listed in Table 3. Debris was introduced into the smaller first-stage cyclone separator as the loose fruits were collected via air suction through the inlet. Heavy loose fruits would then gather via the outlet in the first-stage cyclone separator, while lighter debris was pulled through the vortex finder and collected in the second-stage cyclone separator. Consequently, clean, loose fruits were collected by the first stage cyclone, while undesirable debris was deposited in the second cyclone. Collection efficiency was calculated by comparing the percentage of collected loose fruits from the first cyclone to the total particles introduced from the inlet.

3. Results and discussion

3.1. Flow analysis

In this section, the velocity and pressure profiles of the 20 m/s inlet air speed are presented. Figures 5 and 6 show the velocity and pressure vectors of the dual cyclone separators. Figure 3 illustrates that as air entered the first cyclone, it recorded a high velocity that reached a maximum (red) near the walls. From there, the velocity vectors spiralled into a vortex, with the velocity decreasing as the air descended further. Then, at the bottom of the vortex in the first cyclone, we observed the presence of an inner vortex, where the directions of the velocity vector swirled up to the vortex finder, which led to the second cyclone separator. The same pattern was observed in the second cyclone, where the vectors indicated the presence of inner and outer vortexes. The cyclone separator mechanism theory was confirmed in both dual cyclone separators through the study of velocity vectors. As shown in Figure 6, generally the pressure vectors showed similar patterns in both of the cyclone separators to velocity vectors.

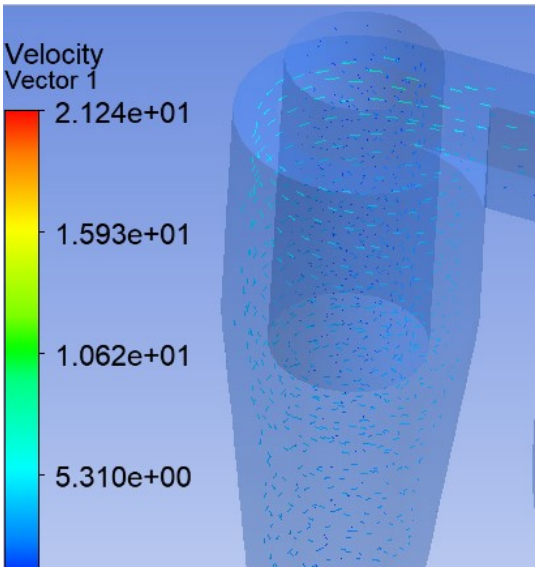

Figure 5. Velocity vectors in dual cyclone separators.

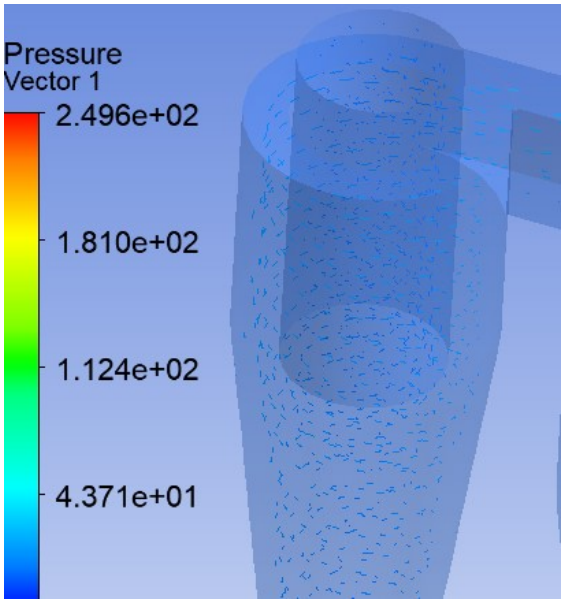

Figure 6. Pressure vectors in dual cyclone separators.

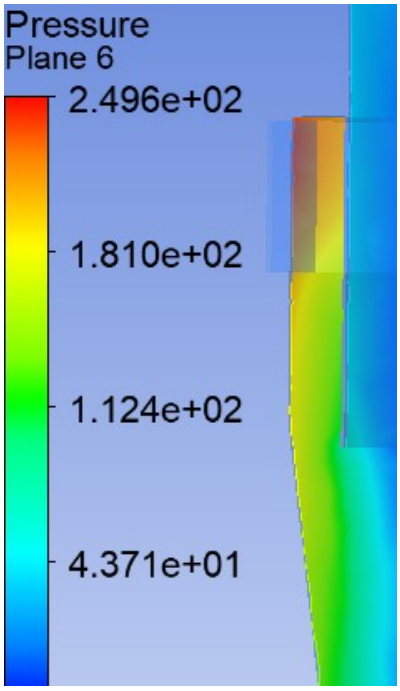

Figure 7. First cyclone pressure profile.

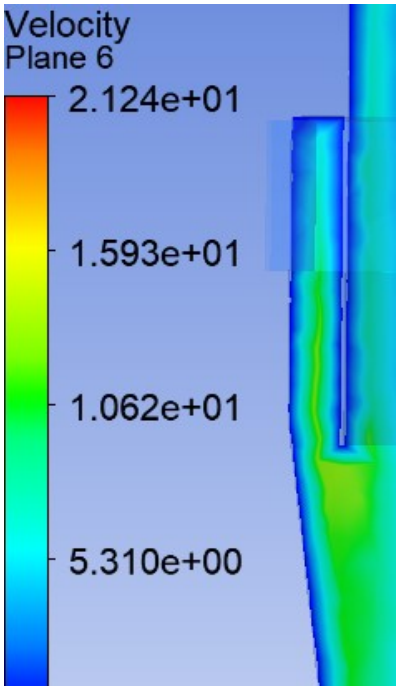

Figure 8. First cyclone velocity profile.

As can be seen from Figures 7 and 8, the profiles for both pressure and velocity were satisfactory, in accordance with the cyclone separator theory. The velocity at the walls, where blue shades were observed, remained stagnant. Additionally, we observed a stagnation flow at the center of the cyclone separator. As the air swirled down the separator along the wall, the center experienced a speed stagnation, while the inner vortex transported lighter material out of the first cyclone. A Rankine vortex that explained the operation of a cyclone was confirmed [34].

3.1. Effect on pressure drop

The pressure drop of a cyclone separator offers excellent indications of a cyclone's performance. A change in pressure drop through variations in cyclone operation will result in its performance directly due to the friction of the fluid and materials with the cyclone walls and internal flow, as explained by [28] in their experimental work and [32] in their theoretical cyclone calculation work. In their theoretical calculations, [32] also demonstrated that the pressure drop of a cyclone separator heavily depends on the cyclone's inlet speed, as the intensely turbulent flow within the cyclone exerts forces on it [35]. In the current study, Figure 9 demonstrates that a significant increase in the machine's inlet air speed led to a dramatic increase in the pressure drop. By increasing the velocity of air intake from 13 m/s to 30 m/s, the pressure drop rose sharply from 207.12 Pa to 1064.48 Pa, while an air intake increase to 46 m/s increased the pressure drop to 2599.21 Pa. On another note, from Figure 10, it is apparent that increasing the inlet air speed from 13 m/s to 30 m/s reduced the collection efficiency by 14.92 % from 80.05% to 66.13 %. On the other hand, a 54.44 % collection was recorded at 46 m/s inlet air speed. Through the analysis of the effects of air inlet speed variations on the pressure drop and collection efficiency of the oil palm loose fruit collector, it is obvious that the lower air intake setting was desirable to achieve higher efficiency. [31] worked cyclone-type variations on the collection of jojoba seeds; it was found that using the 1D2D cyclone records the best

efficiency at 92.8% compared to the 1D3D cyclone with 78.4 %. For further clarification, [32] reported that at the same inlet speed of 11.4 m/s, the 1D2D cyclone and 1D3D cyclone recorded a pressure drop of 349 Pa and 545 Pa, respectively. Thus, it is obvious a lower-pressure cyclone is intended in the case of seed collections such as the oil palm loose fruits and the jojoba seeds. However, it is worth noting that pressure drops recorded do not correlate to the collection efficiencies when different inlet speeds are used. At the same inlet speed, a lower pressure drop led to a higher collection efficiency, as reported by [32]. In contrast, the variations in pressure drops in the present study were caused by the different inlet speeds entirely without the compromise of other factors. Therefore, this clarification dispels the false belief that a higher pressure drop will result in a higher collection efficiency. Instead, the data presented in Figure 9 demonstrates that a higher speed would result in a higher pressure drop on the system due to the turbulent flow within it.

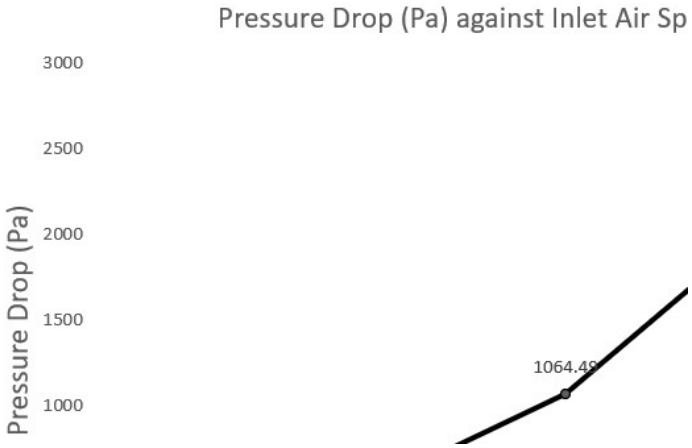

Figure 9. Machine pressure drop against inlet air speed.

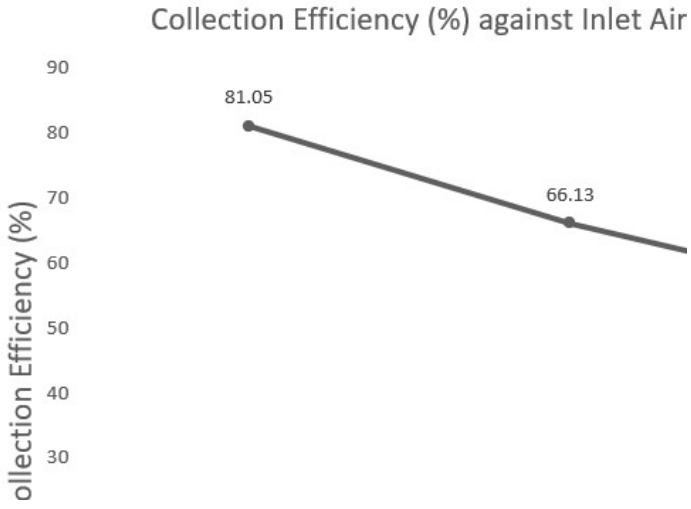

Figure 10. Machine collection efficiency against inlet air speed.

4. Conclusion

In conclusion, a lower air speed is preferred for a more efficient oil palm loose fruit collector. Data trend indicated that increasing the inlet air speed from 13 m/s to 30 m/s lowered the collection efficiency from 80.05% to 66.13%, while a 54.44% collection was recorded at 46 m/s inlet air speed. Besides inlet air speed, there are numerous parameters to take into account for a more efficient loose fruit collector, such as the geometry of vortex diameter, diameter of cyclone exit and cone variations. Thus, a more comprehensive study is needed to assess each parameter and their interactions with one another for an efficient and reliable oil palm loose fruit collector machine.

Acknowledgements

This work was supported by Universiti Teknologi Malaysia (UTM) under the UTM-Matching Grant (Grant Number: Q.J130000.3024.04M81).

Conflict of interest

The authors declare no conflict of interest.

References

[1] Malaysia Palm Oil Board (2023). Oil palm statistics. Area (2023). Retrieved from https://bepi.mpob.gov.my/index.php/area/307-area-2023/1189-oil-palm-planted-area-2023

[2] Yusoff, M. Z. M. (2019). Loose fruit collector machine in Malaysia: A review. *International Journal of Engineering Technology and Sciences*, *6*(2), 65-75. https://doi.org/10.15282/ijets.v6i2.2909

[3] Ruswanto, A., Ramelan, A. H., Praseptiangga, D. and Partha, I. B. B. (2020). Palm oil yield potency on different level of ripening and storage time based on fruits percentage and fresh fruit bunches. IOP Conf. Series: Earth and Environmental Science 443(1), 012005. **DOI** 10.1088/1755-1315/443/1/012005

[4] Darius, E. P. & Fairulnizam, M. H. (2015) Effects of collecting systems and plantation environment on debris accumulation in a collected oil palm loose fruits. *Proc. Int. Conf. Plt. Phy. 2014*, 147-151. ISBN 978-967-10840-4-5

[5] Sime Darby (2008). Loose Fruit vs. Lost Income. Seedlink: A bimonthly publication by Sime Darby Sdn. Bhd., March 2008, Vol. 2/6. Subang Jaya. pp.8.

[6] Shuib, A. R., Khalid, M. R. & Bakri, M. A. M. (2018). Development of oil palm loose fruit collecting machine with elevated discharge mechanism. *International Journal of Engineering Research & Technology.* 7(10), 225-234.

[7] Chang, L. C., Sani, A. R. A., & Basran, Z. (2003). An economic perspective of oil extraction rate in the oil palm industry of Malaysia. *Oil Palm Industry Economic Journal*, *3*(1), 25-31.

[8] Yusoff, M. Z. M., Zamri, A., Abd Kadir, M. Z. A., Hassan, W. W., & Azis, N. (2020). Development of integrated loose fruit collector machine for oil palm plantations. *Bulletin of Electrical Engineering and Informatics*, *9*(2), 500-506. https://doi.org/10.11591/eei.v9i2.2087

[9] Sukadarin, E. H., Deros, B. M., Nawi, N. S. M., Ghani, J. A., Ismail, A. R., & Zakaria, J. (2016). Back pain and the observed factors among oil palm workers. *International Journal Of Engineering Technology and Sciences*, *3*(1), 70-78. https://doi.org/10.15282/ijets.5.2016.1.9.1048

[10] Ahmad, H., Ahmad Zamri, M.Y, & Mohd S. J. (1995). Loose Fruit Collector. PORIM Information Series No.19, Palm Oil Research Institute of Malaysia (PORIM), Selangor.

[11] Khalid, M. R. & Shuib, A. R. (2017). Performance of oil palm loose fruits separating machine. *Journal of Oil Palm Research,* 29 (3), 358-365. . https://doi.org/10.21894/jopr.2017.2903.08

[12] Shuib, A. R. & Khalid, M.R. (2005). Air-Assisted Loose Fruit Separating Machine, MPOB Information Series No.261, Malaysia Palm Oil Board (MPOB), Selangor.
[13] Guo, M., Yang, L., Son, H., Le, D. K., Manickam, S., Sun, X., & Yoon, J. Y. (2024). An overview of novel geometrical modifications and optimizations of gas-particle cyclone separators. *Separation and Purification Technology*, *329*, 125136. https://doi.org/10.1016/j.seppur.2023.125136.
[14] Park, D. & Go, J. (2020). Design of Cyclone Separator Critical Diameter Model Based on Machine Learning and CFD. Processes. 8. 10.3390/pr8111521.
[15] Babaoğlu, N. U., Parvaz, F., Hosseini, S. H., Elsayed, K., & Ahmadi, G. (2021). Influence of the inlet cross-sectional shape on the performance of a multi-inlet gas cyclone. *Powder Technology*, *384*, 82-99. https://doi.org/10.1016/j.powtec.2021.02.008
[16] Gao, Z., Wang, J., Liu, Z., Wei, Y., Wang, J., & Mao, Y. (2020). Effects of different inlet structures on the flow field of cyclone separators. *Powder technology*, *372*, 519-531. https://doi.org/10.1016/j.powtec.2020.06.014
[17] Nassaj, O. R., Toghraie, D., & Afrand, M. (2019). Effects of multi inlet guide channels on the performance of a cyclone separator. *Powder Technology*, *356*, 353-372. https://doi.org/10.1016/j.powtec.2019.08.038
[18] Siadaty, M., Kheradmand, S., & Ghadiri, F. (2017). Study of inlet temperature effect on single and double inlets cyclone performance. *Advanced Powder Technology*, *28*(6), 1459-1473. https://doi.org/10.1016/j.apt.2017.03.015
[19] Misiulia, D., Andersson, A. G., & Lundström, T. S. (2015). Effects of the inlet angle on the flow pattern and pressure drop of a cyclone with helical-roof inlet. *Chemical engineering research and design*, *102*, 307-321. https://doi.org/10.1016/j.cherd.2015.06.036
[20] Misiulia, D., Andersson, A. G., & Lundström, T. S. (2017). Effects of the inlet angle on the collection efficiency of a cyclone with helical-roof inlet. *Powder Technology*, *305*, 48-55. https://doi.org/10.1016/j.powtec.2016.09.050
[21] Li, H. X., Gao, B. G., & Li, B. (2015). Numerical analysis of flow dynamics of cyclone separator used for circulating fluidized bed boiler. *Chemical Engineering Transactions*, *46*, 991-996. https://doi.org/10.3303/CET1546166
[22] Wasilewski, M., Brar, L. S., & Ligus, G. (2020). Experimental and numerical investigation on the performance of square cyclones with different vortex finder configurations. *Separation and Purification Technology*, *239*, 116588. https://doi.org/10.1016/j.seppur.2020.116588
[23] Liu, D., Hsiao, T. C., & Chen, D. R. (2015). Performance study of a miniature quadru-inlet cyclone. *Journal of Aerosol Science*, *90*, 161-168. https://doi.org/10.1016/j.jaerosci.2015.08.010
[24] Elsayed, K. & Lacor, C. (2010). The effect of vortex finder diameter on cyclone separator performance and flow field. *V European Conference on Computational Fluid Dynamics. 14-17 June 2010.*
[25] Ahmad Zamri, M.Y & Ahmad, H. (1999). Mechanical Loose Fruit collector. PORIM Information Series No.57, Palm Oil Research Institute of Malaysia (PORIM), Selangor.
[26] Yusof, MD. Z. A & Yusoff, M. M. Z. (2017). A Motorized Device For Picking And Collecting Loose Fruits. International Publication Number: WO2016072829A1. https://patents.google.com/patent/WO2016072829A1.
[27] Ramdhan, M. K., Rahim, A. S. & Norman, K. (2019). Determination of minimum suction level of collecting oil palm loose fruits. *Konvensyen Kebangsaan Kejuruteraan Pertanian dan Makan 2019, Putrajaya.* pp. 198-201. eISBN 978-967-16145-1-8
[28] Hoekstra, A. J., Derksen, J. J., & Van Den Akker, H. E. A. (1999). An experimental and numerical study of turbulent swirling flow in gas cyclones. *Chemical engineering science*, *54*(13-14), 2055-2065. https://doi.org/10.1016/S0009-2509(98)00373-X
[29] ANSYS FLUENT Theory Guide, ANSYS, Inc., Release 15.0, November 2013.
[30] Morsi, S. A. J., & Alexander, A. J. (1972). An investigation of particle trajectories in two-phase flow systems. *Journal of Fluid mechanics*, *55*(2), 193-208. https://doi.org/10.1017/S0022112072001806

[31] El-Emam, M. A., Zhou, L., Shi, W. & Han, C. (2021). Performance evaluation of standard cyclone separators by using CFD–DEM simulation with realistic bio-particulate matter. *Powder Technology*, 385, 357-374. https://doi.org/10.1016/j.powtec.2021.03.006

[32] Wang, L. (2004). Theoretical study of cyclone design, Doctoral Thesis, Texas A&M University.

[33] Owolarafe, O. K., Olabige, M. T., & Faborode, M. O. (2007). Physical and mechanical properties of two varieties of fresh oil palm fruit. *Journal of Food Engineering*, *78*(4), 1228-1232. https://doi.org/10.1016/j.jfoodeng.2005.12.049

[34] Sakin, A., Karagoz, I., & Avci, A. (2019). Performance analysis of axial and reverse flow cyclone separators. *Chemical Engineering and Processing-Process Intensification*, *144*, 107630. https://doi.org/10.1016/j.cep.2019.107630.

[35] Samadi, M., Mesbah, M., & Majidi, S. (2024). A novel approach to designing compact cyclones for efficient natural gas filtration. *Powder Technology*, 448, 120259. https://doi.org/10.1016/j.powtec.2024.120259